# 自旋轨道耦合诱导的调制不稳定性

翟云佳，陈园园，张永平[*]

上海大学物理系，上海 200444

**摘要**　原子玻色-爱因斯坦凝聚体的调制稳定性决定了凝聚体的超流属性，是超冷原子物理研究的重要内容。在由拉曼光形成的自旋轨道耦合的玻色-爱因斯坦凝聚体中，存在 4 种不同的零动量本征态，由于自旋轨道耦合的存在，其中两种态载有流，另两种态不载流。通过对它们进行调制稳定性分析，发现无论在什么参数空间，这 4 种态都是调制不稳定的，即自旋轨道耦合总是能够诱导出调制不稳定性。这些态的动力学演化揭示调制不稳定性能够产生复杂的图案。

**关键词**　原子与分子物理学；自旋轨道耦合；玻色-爱因斯坦凝聚体；调制不稳定性

**中图分类号**　O431.2　　　　**文献标志码**　A　　　　　　　　　　　　**DOI**：10.3788/AOS230955

## 1　引　　言

调制不稳定性（MI）是非线性动力学的重要现象，在多种系统中得到了广泛研究[1]。该现象是指不稳定性导致具有微小振幅的调制波的自发增长，从而产生了较大振幅的局域波。产生调制不稳定性的核心机制在于系统的固有非线性项和色散之间的相互作用，导致微小扰动不稳定性增长。在调制不稳定性的研究中，一般采用线性稳定性分析和非线性波动方程等数学方法来描述系统的动力学行为和稳定性特性。近年来，人们开始关注超冷原子气体中的玻色-爱因斯坦凝聚体，并开展了很多这方面的研究[2-3]。玻色-爱因斯坦凝聚体也是研究调制不稳定性的极好平台，这是因为该系统中的非线性作用与原子散射长度有关，可以通过实验手段例如光学手段[4]或者费什巴赫（Feshbach）共振[5-7]等进行精细控制。单组分玻色-爱因斯坦凝聚体系统中的调制不稳定性已经得到了广泛研究[8-9]，得到的结论是单组分玻色-爱因斯坦凝聚体仅在吸引非线性相互作用下才可能出现调制不稳定性，且玻色-爱因斯坦凝聚体中的调制不稳定性可以用于孤子形成的研究。与单组分系统相比，两组分玻色-爱因斯坦凝聚体具有更多新奇的物理特性。当组分之间的相互作用强于组分内部的相互作用时，均匀的两组分玻色-爱因斯坦凝聚体会表现出相分离不稳定性[10-11]。此外，如果存在线性耦合，两个组分之间会出现拉比振荡，并且可能会改变相分离不稳定性的临界条件，目前已经在实验[12]中观察到耦合诱导的动力学现象。在两组分玻色-爱因斯坦凝聚体中，戈尔茨坦小组[13]最早考虑了空间不稳定性和调制不稳定性的可能性。随后的研究表明，在两组分玻色-爱因斯坦凝聚体系统中，即使存在排斥相互作用，也可能存在调制不稳定性[14-15]。当组分间排斥相互作用比组分内排斥相互作用更强时，调制不稳定性会诱导多域的产生[16-17]。最近，关于调制不稳定性的研究结果也表明，具有自旋轨道耦合的玻色-爱因斯坦凝聚体受到了比以往更多的关注[18-26]，这是因为引入自旋轨道耦合可以扩展传统的玻色-爱因斯坦凝聚体的调制不稳定参数区域，从而使其具有更多新奇的性质。

除此之外，研究者对于具有零动量的特定态的动力学不稳定性存在着极大的兴趣[26-28]。在不存在自旋轨道耦合的玻色-爱因斯坦凝聚体系统中，原子会凝结成零动量态。同时，由于态的准动量为零，自旋轨道耦合本身对零动量态没有影响，但自旋轨道耦合的存在确实使零动量态变得不稳定。Wang 等[27]最早揭示了零动量态下自旋轨道耦合引起的动力学不稳定性。

本文探讨了具有由拉曼光产生的自旋轨道耦合的一维两组分玻色-爱因斯坦凝聚体系统的调制不稳定性，发现该系统存在 4 种不同的零动量态，其中两种载有流，另两种不载流。文献[19-28]只是针对其中一种不载流的零动量态进行了稳定性分析。本文对所有的零动量态进行稳定性分析，发现在所有的参数空间中，这些态都是调制不稳定的。考虑到没有自旋轨道耦合后，这些态都是稳定的，因此将这些态的不稳定性称为"自旋轨道耦合诱导的调制不稳定性"。作为不稳定性的一个重要应用，通过动力学演化这些零动量态，发现调制不稳定性可以激发出复杂的图案。

## 2 理论模型

研究系统是一个具有自旋轨道耦合的一维两组分玻色-爱因斯坦凝聚体,该自旋轨道耦合由拉曼激光耦合原子能级形成。它可以由格罗斯-皮塔耶夫斯基方程(GPEs)来描述:

$$i\frac{\partial \boldsymbol{\Psi}}{\partial t}=\frac{p_x^2}{2}\boldsymbol{\Psi}+\left(\Omega\sigma_x+\gamma p_x\sigma_z\right)\boldsymbol{\Psi}+H_n\boldsymbol{\Psi},\quad(1)$$

式中:旋量波函数为 $\boldsymbol{\Psi}(x,t)=[\Psi_1(x,t),\Psi_2(x,t)]^{\mathrm{T}}$,这里 $\Psi_1$ 和 $\Psi_2$ 分别表示两组分的波函数;$p_x=-i\partial/\partial x$ 为沿着 $x$ 方向的动量算符;$(\sigma_x,\sigma_z)$ 表示标准的泡利自旋矩阵;$\Omega$ 表示拉比耦合强度;$\gamma p_x\sigma_z$ 为一维自旋轨道耦合形式,$\gamma$ 为强度。在 GPEs 中,平均场相互作用可以用 $H_n$ 来描述:

$$H_n=\begin{pmatrix} g\left|\Psi_1\right|^2+g_{12}\left|\Psi_2\right|^2 & 0 \\ 0 & g_{12}\left|\Psi_1\right|^2+g\left|\Psi_2\right|^2 \end{pmatrix},(2)$$

式中:$g$ 和 $g_{12}$ 分别为组分内和组分间的相互作用系数,二者都与 S 波散射长度成正比。方程(1)是无量纲的,以便于数值计算。由于系统的空间分布是均匀的,因此方程(1)中的稳定解具有如下平面波形式:

$$\boldsymbol{\Psi}(x,t)=\exp\left(-i\mu t+ik_x x\right)\begin{pmatrix}\phi_1 \\ \phi_2\end{pmatrix},\quad(3)$$

式中:$\mu$ 为化学势;$k_x$ 为沿 $x$ 方向的准动量;自旋布居数满足 $|\phi_1|^2+|\phi_2|^2=1$。将平面波解代入方程(1)后,可以得到非线性色散关系 $\mu(k_x)$ 和相应的本征态。

这些平面波解的调制不稳定性可以从 Bogoliubov de Gennes (BdG)方程中得到检验。在将扰动添加到方程(3)的平面波解后,得到

$$\boldsymbol{\Psi}(x,t)=\exp(-i\mu t+ik_x x)\times\begin{pmatrix}\phi_1+U_1\exp(iq_x x-i\omega t)+V_1^*\exp(-iq_x x+i\omega^* t) \\ \phi_2+U_2\exp(iq_x x-i\omega t)+V_2^*\exp(-iq_x x+i\omega^* t)\end{pmatrix},\quad(4)$$

式中:$U_{1,2}$ 和 $V_{1,2}$ 为微扰振幅;$\omega$ 为微扰能量;$q_x$ 为沿 $x$ 方向的微扰准动量。将式(4)代入方程(1)并保留扰动振幅的线性项,得到以下 BdG 方程:

$$\omega\begin{pmatrix}U_1 \\ V_1 \\ U_2 \\ V_2\end{pmatrix}=H_{\mathrm{BdG}}\begin{pmatrix}U_1 \\ V_1 \\ U_2 \\ V_2\end{pmatrix}。\quad(5)$$

BdG 哈密顿量为

$$H_{\mathrm{BdG}}=\begin{pmatrix} \mathcal{L}_1+\gamma q_x & g\phi_1^2 & \Omega+g_{12}\phi_1\phi_2^* & g_{12}\phi_1\phi_2 \\ -g\phi_1^{*2} & -\mathcal{L}_1+\gamma q_x & -g_{12}\phi_1^*\phi_2^* & -\Omega-g_{12}\phi_1^*\phi_2 \\ \Omega+g_{12}\phi_1^*\phi_2 & g_{12}\phi_1\phi_2 & \mathcal{L}_2-\gamma q_x & g\phi_2^2 \\ -g_{12}\phi_1^*\phi_2^* & -\Omega-g_{12}\phi_1\phi_2^* & -g\phi_2^{*2} & -\mathcal{L}_2-\gamma q_x \end{pmatrix},\quad(6)$$

$$\mathcal{L}_1=\frac{1}{2}q_x^2-\mu+2g\left|\phi_1\right|^2+g_{12}\left|\phi_2\right|^2,\quad(7)$$

$$\mathcal{L}_2=\frac{1}{2}q_x^2-\mu+2g\left|\phi_2\right|^2+g_{12}\left|\phi_1\right|^2。\quad(8)$$

BdG 哈密顿量是非厄米的,因此会出现复数本征值。对于方程(3)中给定的态,如果 BdG 方程的 $\omega$ 具有复数模,则该状态是调制不稳定的。当出现复数模时,方程(4)中的扰动会呈指数增长并破坏状态的性质。

本文主要研究准动量为零的态,通过 BdG 方程的计算,揭示其总是具有调制不稳定性的原因。之所以对零动量态感兴趣,是因为所提出的自旋轨道耦合诱导的调制不稳定性总是对于这些零动量态成立。它具有的调制不稳定性使得位置空间展现出复杂的图案结构动力学,且由于自旋轨道耦合存在的影响,系统两个组分的波函数在动量空间中的分布也会受到一定影响。本文展示了方程(1)随时间演化形成的非线性动力学图案,选择的初始状态为零动量态加上随机分布的微扰,形式为 $\Psi_{1,2}(x,t=0)=\phi_{1,2}(1+0.01R)$,其中,$R$ 为随机扰动。时间演化是通过标准的分步傅里叶方法来实现的,数值模拟的空间尺度为 $x\in[-200,200]$。

## 3 结果与分析

尽管自旋轨道耦合的存在使得零准动量态不稳定,但是方程(3)的平面波解动量态的存在并不取决于自旋轨道耦合。将方程(3)中的零准动量态代入 GPEs 中,得到

$$\begin{cases}\mu\phi_1=\left(g\left|\phi_1\right|^2+g_{12}\left|\phi_2\right|^2\right)\phi_1+\Omega\phi_2 \\ \mu\phi_2=\left(g\left|\phi_2\right|^2+g_{12}\left|\phi_1\right|^2\right)\phi_2+\Omega\phi_1\end{cases}。\quad(9)$$

结合上述方程与归一化条件 $|\phi_1|^2+|\phi_2|^2=1$ 求解,可得到 4 种不同的零准动量态,分别为

$$
\begin{pmatrix} \psi_1 \\ \psi_2 \\ \mu \\ J \end{pmatrix} = \begin{pmatrix} \dfrac{1}{\sqrt{2}} \\ \dfrac{1}{\sqrt{2}} \\ \dfrac{g+g_{12}}{2}+\Omega \\ 0 \end{pmatrix}, \begin{pmatrix} \dfrac{1}{\sqrt{2}} \\ -\dfrac{1}{\sqrt{2}} \\ \dfrac{g+g_{12}}{2}-\Omega \\ 0 \end{pmatrix}, \begin{pmatrix} \dfrac{f_1}{\sqrt{1+f_1^2}} \\ \dfrac{1}{\sqrt{1+f_1^2}} \\ \dfrac{g+g_{12}}{2}+\Omega\dfrac{1+f_1^2}{2f_1} \\ \gamma\dfrac{f_1^2-1}{f_1^2+1}\boldsymbol{e}_x \end{pmatrix}, \begin{pmatrix} \dfrac{f_2}{\sqrt{1+f_2^2}} \\ \dfrac{1}{\sqrt{1+f_2^2}} \\ \dfrac{g+g_{12}}{2}+\Omega\dfrac{1+f_2^2}{2f_2} \\ \gamma\dfrac{f_2^2-1}{f_2^2+1}\boldsymbol{e}_x \end{pmatrix}, \tag{10}
$$

式中：$f_{1(2)}=\dfrac{g-g_{12}}{2\Omega}\pm\dfrac{1}{2}\sqrt{\left(\dfrac{g-g_{12}}{\Omega}\right)^2-4}$；$\boldsymbol{e}_x$ 为 $x$ 方向的单位矢量。零动量态携带流的定义为

$$
J=<\boldsymbol{\Psi}|\hat{v}|\boldsymbol{\Psi}>=\gamma<\boldsymbol{\Psi}|\sigma_z|\boldsymbol{\Psi}>\boldsymbol{e}_x=\gamma(\psi_1^2-\psi_2^2)\boldsymbol{e}_x, \tag{11}
$$

式中：$\hat{v}$ 为速度算符。从式（10）看到，前两种零动量态不携带流，后两种零动量态携带流。在先前的研究中，已对第一种无载流态进行了调制不稳定性和非线性动力学研究[19-28]，而从是否载流的角度分析，第二种态和第一种态属于同一类，因此本文后续的研究将集中在后两种载流态的调制不稳定性相关性质，即如下的零动量态：

$$
\begin{pmatrix} \psi_1 \\ \psi_2 \\ \mu \\ J \end{pmatrix} = \begin{pmatrix} \dfrac{f_1}{\sqrt{1+f_1^2}} \\ \dfrac{1}{\sqrt{1+f_1^2}} \\ \dfrac{g+g_{12}}{2}+\Omega\dfrac{1+f_1^2}{2f_1} \\ \gamma\dfrac{f_1^2-1}{f_1^2+1}\boldsymbol{e}_x \end{pmatrix}, \begin{pmatrix} \dfrac{f_2}{\sqrt{1+f_2^2}} \\ \dfrac{1}{\sqrt{1+f_2^2}} \\ \dfrac{g+g_{12}}{2}+\Omega\dfrac{1+f_2^2}{2f_2} \\ \gamma\dfrac{f_2^2-1}{f_2^2+1}\boldsymbol{e}_x \end{pmatrix}。 \tag{12}
$$

该态存在的条件为 $|g-g_{12}|\geqslant 2\Omega$，也就是载流态

的存在性取决于非线性效应，和自旋轨道耦合本身没有关系。接下来，在所有的参数空间中展示自旋轨道耦合带来的调制不稳定性。下文将会对两类典型的参数进行分析，在这两类参数下，载流态调制不稳定性的具体表现形式有所不同。

### 3.1　$g=1$、$g_{12}=0.2$、$\Omega=0.2$、$\gamma=1$

本节展示了参数范围内的载流零动量态的调制不稳定性。首先，将两个在 $g=1$、$g_{12}=0.2$、$\Omega=0.2$ 情况下存在的载流零动量态代入 BdG 方程。如果 $\omega$ 的虚部不为零，则系统具有调制不稳定性。

图 1 展示了扰动准动量 $q_x$ 和 $\omega$ 的虚部最大绝对值 $\xi$ 的演化图像，其中 $\xi=\max(|\mathrm{Im}[\omega]|)$。可以看到，两个载流态具有相同的调制不稳定性。与此同时，当存在拉比耦合时，系统的组分内相互作用系数大于组分间相互作用系数，调制不稳定性图像具有 4 个分支。分布于较小准动量附近的 2 个分支具有同等贡献，称为主调制不稳定性带；处于较大准动量附近的 2 个分支，称为次调制不稳定性带。当 2 种非线性相互作用都是排斥相互作用时，研究调制不稳定性会具有一定的困难，这是因为两种相互作用都是排斥的，对于调制不稳定性不具有贡献。但是自旋轨道耦合的存在，为玻色-爱因斯坦凝聚体系统带来了一种新的调制不稳定性的状态。图 2 表明，在自旋轨道耦合的帮助下，载流零动量态的调制不稳定性仍然可能存在。
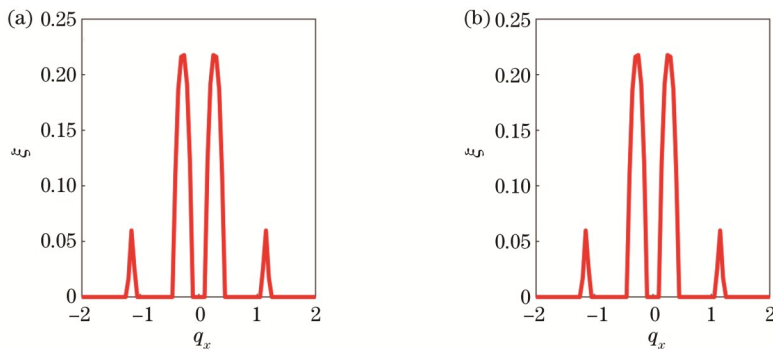


图 1　当 $g=1$、$g_{12}=0.2$、$\Omega=0.2$、$\gamma=1$时，调制不稳定性的增益图像。(a)$f_1=3.7321$；(b)$f_2=0.2679$

Fig. 1　Gain images of the MI for $g=1$, $g_{12}=0.2$, $\Omega=0.2$, and $\gamma=1$. (a)$f_1=3.7321$；(b)$f_2=0.2679$

图 2 和图 3 所示分别为当 $g=1$、$g_{12}=0.2$、$\Omega=0.2$、$\gamma=1$时，调制不稳定性诱导的时间演化图像。尽
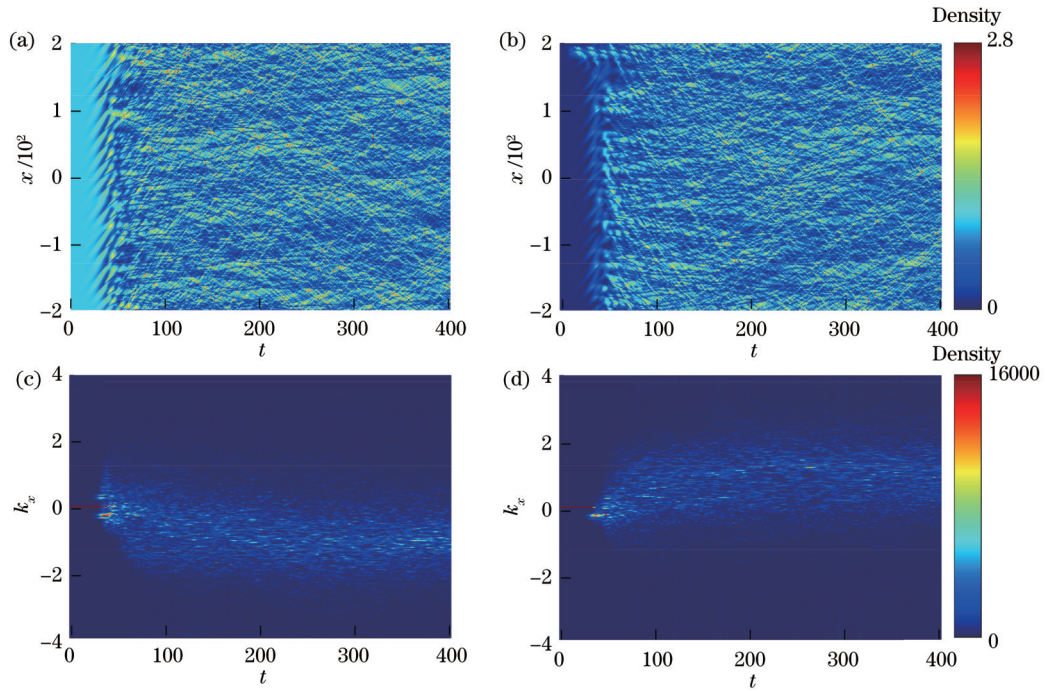
管初态的密度分布不同，导致图 2 和图 3 中的两个组分演化的密度大小不完全相同，但是两个组分的密度演

图 2　当 $g=1$、$g_{12}=0.2$、$\Omega=0.2$、$\gamma=1$、$f_1=3.7321$ 时，零准动量态的时间演化图像。(a)$n_1=|\psi_1(x)|^2$ 和(b)$n_2=|\psi_2(x)|^2$ 时位置空间的两个组分密度的演化图像；(c)$n_1=|\psi_1(k)|^2$ 和(d)$n_2=|\psi_2(k)|^2$ 时准动量空间两个组分密度的演化图像

Fig. 2　Time evolution of zero-quasimomentum states for $g=1$, $g_{12}=0.2$, $\Omega=0.2$, $\gamma=1$, and $f_1=3.7321$. Density evolution of two components in coordinate space with (a) $n_1=|\psi_1(x)|^2$ and (b) $n_2=|\psi_2(x)|^2$; density evolution of two components in quasimomentum space with (c) $n_1=|\psi_1(k)|^2$ and (d) $n_2=|\psi_2(k)|^2$
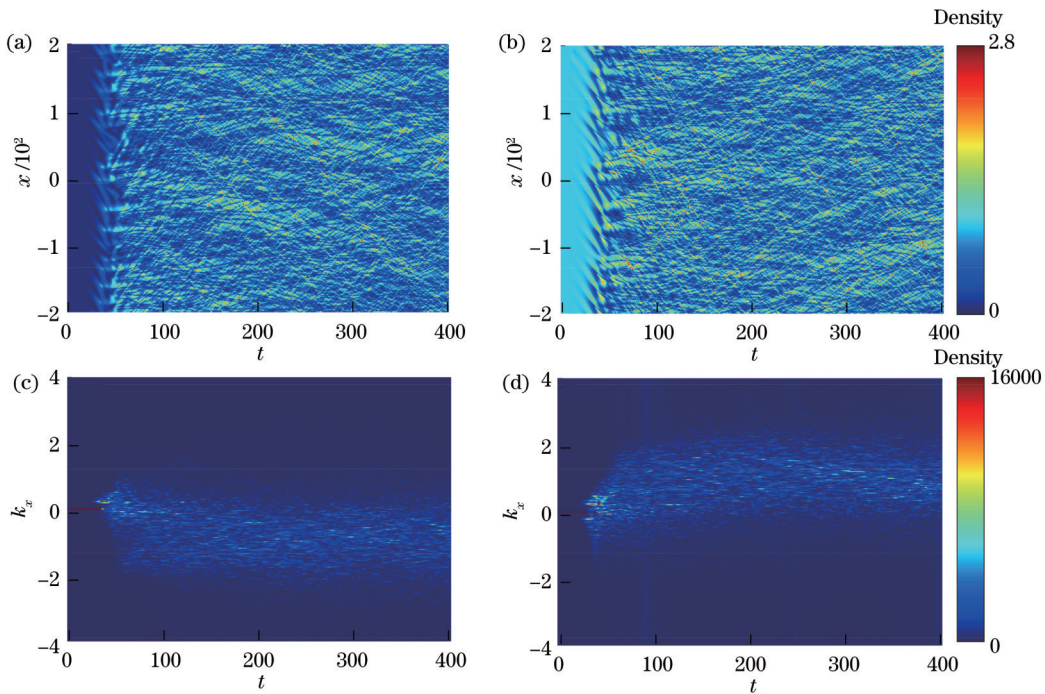


图 3　当 $g=1$、$g_{12}=0.2$、$\Omega=0.2$、$\gamma=1$、$f_2=0.2679$ 时，零准动量态的时间演化图像。(a)$n_1=|\psi_1(x)|^2$ 和(b)$n_2=|\psi_2(x)|^2$ 时位置空间的两个组分密度的演化图像；(c)$n_1=|\psi_1(k)|^2$ 和(d)$n_2=|\psi_2(k)|^2$ 时准动量空间两个组分密度的演化图像

Fig. 3　Time evolution of zero-quasimomentum states for $g=1$, $g_{12}=0.2$, $\Omega=0.2$, $\gamma=1$, and $f_2=0.2679$. Density evolution of two components in coordinate space with (a) $n_1=|\psi_1(x)|^2$ and (b) $n_2=|\psi_2(x)|^2$; density evolution of two components in quasimomentum space with (c) $n_1=|\psi_1(k)|^2$ and (d) $n_2=|\psi_2(k)|^2$

化行为相似，并且分别具有向 $x$ 轴正方向与负方向运动的趋势。随着时间的推移，特别是在 $t=50$ 后，两种组分都持续地进行混沌振荡。在准动量空间中的波函数动力学中，可以进一步看到两种组分有不同的运动

趋势且关于 $k_x$ 轴保持反转对称性。演化一定时间后，两种组分均分解成较小的局域分布，在准动量空间的正负区域显示出明显的分离。这是因为演化初期由主调制不稳定带主导，导致准动量空间的密度分布趋向于主调制不稳定带所在的准动量空间，而随着演化时间的延长，准动量空间的波函数分布逐渐传播到次调制不稳定带，最后趋于次调制不稳定带的准动量空间附近并进行混沌传播。

**3.2 $g=1$、$g_{12}=1.8$、$\Omega=0.2$、$\gamma=1$**

本节展示 $g=1$、$g_{12}=1.8$、$\Omega=0.2$ 时，载流零动量态的调制不稳定性。由 3.1 节可知：当 $g=1$、$g_{12}=0.2$、$\Omega=0.2$ 时，系统的调制不稳定性图像会出现 4 个

分支，分别是分布于较小准动量附近的主调制不稳定性带和分布于较大准动量附近的次调制不稳定性带；从位置空间和准动量空间的态密度演化图像发现，演化图像与调制不稳定性图像有较好的一致性。但是在分析后发现，在保持自旋轨道耦合强度、拉比耦合强度和 $g$ 不变的情况下，改变 $g_{12}$ 的大小，使得 $g<g_{12}$，会使得调制不稳定性图像只存在两个分支，即主调制不稳定性带，而次调制不稳定性带消失了（图 4）。这可以理解为组分间的排斥作用增大，使得两个不稳定性分支进行合并，留下占主导的主调制不稳定性带，且此时的主调制不稳定性带相较于图 1，占据的准动量空间分布更大。



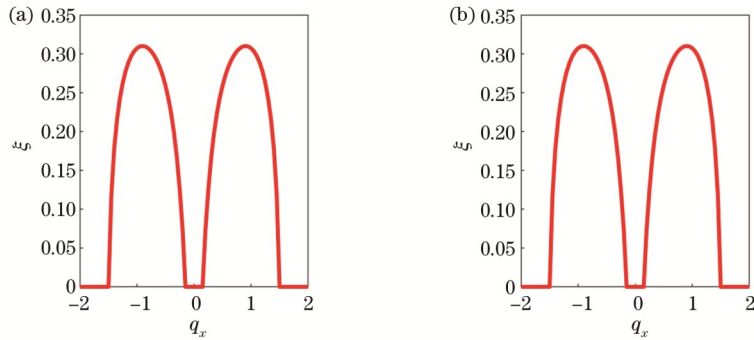图 4 当 $g=1$、$g_{12}=1.8$、$\Omega=0.2$、$\gamma=1$ 时，调制不稳定性的增益图像。(a) $f_1=-0.2679$；(b) $f_2=-3.7321$
Fig. 4 Gain images of the MI for $g=1$, $g_{12}=1.8$, $\Omega=0.2$, and $\gamma=1$. (a) $f_1=-0.2679$；(b) $f_2=-3.7321$

为了验证这一分布的准确性，对 $g=1$、$g_{12}=1.8$、$\Omega=0.2$、$\gamma=1$ 时的载流零动量态进行时间演化分析，
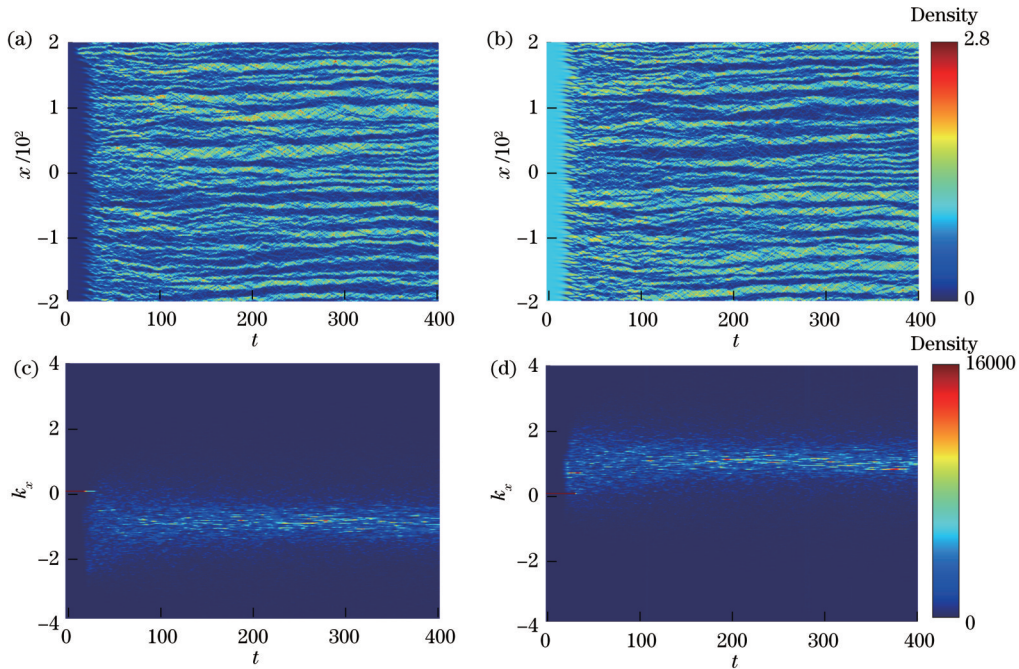
结果如图 5 和图 6 所示。可以看到，由于次调制不稳定性带消失，位置空间分布波函数密度演化图像虽然仍



图 5 当 $g=1$、$g_{12}=1.8$、$\Omega=0.2$、$\gamma=1$、$f_1=-0.2679$ 时，零准动量态的时间演化图像。(a)$n_1=|\psi_1(x)|^2$ 和 (b)$n_2=|\psi_2(x)|^2$ 时位置空间的两个组分密度的演化图像；(c)$n_1=|\psi_1(k)|^2$ 和 (d)$n_2=|\psi_2(k)|^2$ 时准动量空间两个组分密度的演化图像
Fig. 5 Time evolution of zero-quasimomentum states for $g=1$, $g_{12}=1.8$, $\Omega=0.2$, $\gamma=1$, and $f_1=-0.2679$. Density evolution of two components in coordinate space with (a) $n_1=|\psi_1(x)|^2$ and (b) $n_2=|\psi_2(x)|^2$; density evolution of two components in quasimomentum space with (c) $n_1=|\psi_1(k)|^2$ and (d) $n_2=|\psi_2(k)|^2$

有向 $x$ 轴正方向与负方向运动的趋势,但相较于图1,运动趋势变得相对不明显,且波函数进行混沌振荡的时间有所提前,大概在 $t=20$ 后就能被观察到。同时,图5与图6所示的两个组分演化密度大小不完全相同,这是由初态密度分布不同导致的。对准动量空间的波函数演化进行分析,也可以发现两种组分有不同的运动趋势且关于 $k_x$ 轴保持反转对称性,并随着时间的延长,产生较小的局域分布,在准动量空间的正负

区域显示出明显的分离。这种现象的产生机制与3.1节相同,也是因为调制不稳定性的存在,使得波函数动力学演化受到影响,进而让准动量空间的密度分布趋向于主调制不稳定带所在的准动量空间。与3.1节不同的是,此时调制不稳定性的分支仅有两支,即主调制不稳定性带,因此波函数开始混沌振荡后,始终保持在主调制不稳定性带的准动量空间附近。
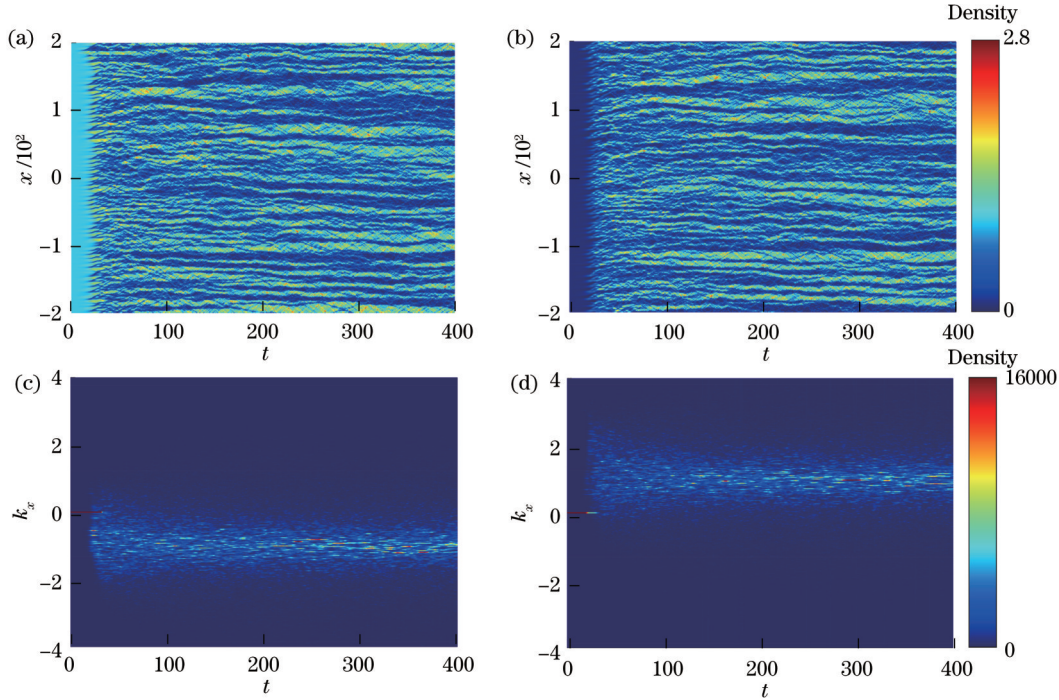


图 6　当 $g=1$、$g_{12}=1.8$、$\Omega=0.2$、$\gamma=1$、$f_2=-3.7321$ 时,零准动量态的时间演化图像。(a)$n_1=|\psi_1(x)|^2$ 和(b)$n_2=|\psi_2(x)|^2$ 时位置空间的两个组分密度的演化图像;(c)$n_1=|\psi_1(k)|^2$ 和(d)$n_2=|\psi_2(k)|^2$ 时准动量空间两个组分密度的演化图像

Fig. 6　Time evolution of zero-quasimomentum states for $g=1$, $g_{12}=1.8$, $\Omega=0.2$, $\gamma=1$, and $f_2=-3.7321$. Density evolution of two components in coordinate space with (a) $n_1=|\psi_1(x)|^2$ and (b) $n_2=|\psi_2(x)|^2$; density evolution of two components in quasimomentum space with (c) $n_1=|\psi_1(k)|^2$ and (d) $n_2=|\psi_2(k)|^2$

## 4　结　　论

　　研究了在具有自旋轨道耦合的一维两组分玻色-爱因斯坦凝聚体的调制不稳定性及其导致的动力学图案,发现存在拉比耦合且满足 $|g-g_{12}|\geqslant 2\Omega$ 的情况下,系统存在4种不同的零动量态,其中2种态携带流,另外2种态不携带流。这4种态的产生并不是由自旋轨道耦合决定的,但是自旋轨道耦合确实影响了系统的调制不稳定性。特别研究了载流零动量态的调制不稳定性,发现:当存在拉比耦合,且组分内相互作用大于组分间相互作用时,调制不稳定性图像会具有4个分支,分别为两个主调制不稳定性带和两个次调制不稳定性带;当组分内相互作用小于组分间相互作用时,调制不稳定性图像则只有两个分支。此外,调制不稳定性与系统的非线性动力学演化图案有良好的一致性,说明调制不稳定性可以激发复杂图案。

## 参 考 文 献

[1] Zakharov V E, Ostrovsky L A. Modulation instability: the beginning[J]. Physica D, 2009, 238(5): 540-548.

[2] 夏佳惠, 李芳, 邓书金, 等. 冷原子高分辨率原位成像系统设计与测试[J]. 激光与光电子学进展, 2022, 59(2): 0222001.
Xia J H, Li F, Deng S J, et al. Design and test of high-resolution imaging system for ultracold atoms[J]. Laser & Optoelectronics Progress, 2022, 59(2): 0222001.

[3] 李文文, 刘乾, 梁昂昂, 等. 空间超冷原子实验两维磁光阱系统的集成设计与实现[J]. 中国激光, 2022, 49(11): 1112001.
Li W W, Liu Q, Liang A A, et al. Integrated design and implementation of two-dimensional magneto-optical trap system for space ultra-cold atom experiment[J]. Chinese Journal of Lasers, 2022, 49(11): 1112001.

[4] Nicholson T L, Blatt S, Bloom B J, et al. Optical Feshbach resonances: field-dressed theory and comparison with experiments[J]. Physical Review A, 2015, 92(2): 022709.

[5] Chin C, Grimm R, Julienne P, et al. Feshbach resonances in ultracold gases[J]. Reviews of Modern Physics, 2010, 82(2): 1225-1286.

[6] Stenger J, Inouye S, Andrews M R, et al. Strongly enhanced inelastic collisions in a Bose-Einstein condensate near Feshbach resonances[J]. Physical Review Letters, 1999, 82(12): 2422-2425.

[7] Cornish S L, Claussen N R, Roberts J L, et al. Stable 85Rb Bose-Einstein condensates with widely tunable interactions[J]. Physical Review Letters, 2000, 85(9): 1795-1798.

[8] Theocharis G, Rapti Z, Kevrekidis P G, et al. Modulational instability of Gross-Pitaevskii-type equations in 1+1 dimensions [J]. Physical Review A, 2003, 67(6): 063610.

[9] Salasnich L, Parola A, Reatto L. Modulational instability and complex dynamics of confined matter-wave solitons[J]. Physical Review Letters, 2003, 91(8): 080405.

[10] Law C K, Pu H, Bigelow N P, et al. "Stability signature" in two-species dilute Bose-Einstein condensates[J]. Physical Review Letters, 1997, 79(17): 3105-3108.

[11] Timmermans E. Phase separation of Bose-Einstein condensates [J]. Physical Review Letters, 1998, 81(26): 5718-5721.

[12] Nicklas E, Strobel H, Zibold T, et al. Rabi flopping induces spatial demixing dynamics[J]. Physical Review Letters, 2011, 107(19): 193001.

[13] Goldstein E V, Meystre P. Quasiparticle instabilities in multicomponent atomic condensates[J]. Physical Review A, 1997, 55(4): 2935-2940.

[14] Kasamatsu K, Tsubota M. Multiple domain formation induced by modulation instability in two-component Bose-Einstein condensates[J]. Physical Review Letters, 2004, 93(10): 100402.

[15] Kasamatsu K, Tsubota M. Modulation instability and solitary-wave formation in two-component Bose-Einstein condensates[J]. Physical Review A, 2006, 74: 013617.

[16] Wen L, Liu W M, Cai Y Y, et al. Controlling phase separation of a two-component Bose-Einstein condensate by confinement [J]. Physical Review A, 2012, 85(4): 043602.

[17] Vidanović I, van Druten N J, Haque M. Spin modulation instabilities and phase separation dynamics in trapped two-component Bose condensates[J]. New Journal of Physics, 2013, 15(3): 035008.

[18] Eto Y, Takahashi M, Kunimi M, et al. Nonequilibrium dynamics induced by miscible-immiscible transition in binary Bose-Einstein condensates[J]. New Journal of Physics, 2016, 18(7): 073029.

[19] Bhat I A, Mithun T, Malomed B A, et al. Modulational instability in binary spin-orbit-coupled Bose-Einstein condensates [J]. Physical Review A, 2015, 92(6): 063606.

[20] Bhuvaneswari S, Nithyanandan K, Muruganandam P, et al. Modulation instability in quasi-two-dimensional spin-orbit coupled Bose-Einstein condensates[J]. Journal of Physics B: Atomic, Molecular and Optical Physics, 2016, 49(24): 245301.

[21] Congy T, Kamchatnov A M, Pavloff N. Nonlinear waves in coherently coupled Bose-Einstein condensates[J]. Physical Review A, 2016, 93(4): 043613.

[22] Li X X, Cheng R J, Zhang A X, et al. Modulational instability of Bose-Einstein condensates with helicoidal spin-orbit coupling [J]. Physical Review E, 2019, 100(3): 032220.

[23] Singh D, Parit M K, Raju T S, et al. Modulational instability in a one-dimensional spin–orbit coupled Bose-Bose mixture[J]. Journal of Physics B, 2020, 53(24): 245001.

[24] Li G Q, Chen G D, Peng P, et al. Modulation instability of a spin-1 Bose-Einstein condensate with spin-orbit coupling[J]. Journal of Physics B, 2017, 50(23): 235302.

[25] Otlaadisa P, Tabi C B, Kofané T C. Modulation instability in helicoidal spin-orbit coupled open Bose-Einstein condensates[J]. Physical Review E, 2021, 103(5): 052206.

[26] Mithun T, Kasamatsu K. Modulation instability associated nonlinear dynamics of spin-orbit coupled Bose-Einstein condensates[J]. Journal of Physics B, 2019, 52(4): 045301.

[27] Wang C J, Gao C, Jian C M, et al. Spin-orbit coupled spinor Bose-Einstein condensates[J]. Physical Review Letters, 2010, 105(16): 160403.

[28] Tabi C B, Otlaadisa P, Kofané T C. Modulation instability of two-dimensional Bose-Einstein condensates with helicoidal and a mixture of Rashba-Dresselhaus spin-orbit couplings[J]. Physics Letters A, 2022, 449: 128334.

# Spin-Orbit-Coupling-Induced Modulation Instability

## Zhai Yunjia, Chen Yuanyuan, Zhang Yongping[*]

*Department of Physics, Shanghai University, Shanghai 200444, China*

## Abstract

**Objective** Modulation instability is a crucial phenomenon in the study of nonlinear dynamics, where an unstable system results in the destruction of its original states, accompanied by the rapid growth of small perturbation instabilities. The Bose-Einstein condensate serves as an ideal platform for exploring modulation instability due to its precise experimental control over the system's nonlinear dynamics. Therefore, studying modulation instabilities holds profound significance in comprehending the nature of Bose-Einstein condensate systems. In this paper, we reveal that spin-orbit coupling can always introduce modulation instability into a kind of specific state. We call it spin-orbit-coupling-induced modulation instability. The states are specific as they are zero-quasimomentum states. We find that there exist four different zero-quasimomentum states, and we classify them as no-current-carrying states and current-carrying states according to whether the states carry current or not. In literature, modulation instability of the no-current-carrying states has been investigated. The current-carrying states are unique due to their current originating from spin-orbit coupling, and their existence is unstable due to nonlinearity. We find that all these zero-quasimomentum states are modulationally unstable in all parameter regimes. The consequence of such modulation instability is the formation of complex wave structures.

**Methods**    The properties of modulation instability and the corresponding nonlinear dynamic images are primarily investigated using Bogoliubov de Gennes (BdG) instability analysis and the split step Fourier method. BdG instability analysis is a widely employed technique for analyzing instability in the study of superfluidity and Bose-Einstein condensates. It primarily examines the system's stability and its response to perturbations by solving nonlinear eigenvalue equations. By diagonalizing the BdG Hamiltonian matrix, the eigenvalues can be obtained. The eigenvalues of the matrix may be complex due to the non-Hermitian nature of the BdG Hamiltonian. If one or more complex numbers exist in the eigenvalues, the state becomes unstable. Consequently, any imposed disturbance experiences exponential growth, leading to the instability of the state. In addition, the split step Fourier method is commonly used for handling time evolution. The underlying principle of this method is to separate the terms of the system Hamiltonian and process them individually. The key step involves employing distinct treatments for the nonlinear and linear terms of the equation to be solved.

**Results and Discussions**    Initially, we investigate the case of $g > g_{12}$ and observe that the system exhibits a four-band modulation instability image in Fig. 1. Among these bands, the two branches positioned near the lower quasi-momentum region are referred to as the primary modulation instability band, while the two branches near the higher quasi-momentum region are known as the secondary modulation instability band. Notably, it is determined that identical chemical potentials of the two current-carrying states yield the same modulation instability image. Furthermore, we perform calculations to ascertain the nonlinear dynamic images (Figs. 2 and 3). The investigation reveals that the density evolution of the two components follows similar ways, exhibiting trends of movement in both positive and negative directions along the $x$-axis. As time progresses, both components undergo chaotic oscillations. In the quasi-momentum space, distinct motion trends and reversal symmetry are observed between the two components. After a certain period of evolution, significant separation occurs. This phenomenon arises from the modulation instability being predominantly influenced by different modulation instability bands at various stages. Initially, the primary modulation instability band dominates, while in later stages, the secondary modulation instability band takes control. Ultimately, the system tends to approach the quasi-momentum space of the secondary modulation instability band, leading to chaotic propagation. Simultaneously, we also examine the scenario where $g < g_{12}$ and observe that the system's modulation instability image consists of only two bands (Fig. 4): the primary modulation instability band. This disappearance of the secondary modulation instability band occurs as the repulsive interaction between the components intensifies, causing the two unstable branches to merge. Following a nonlinear dynamic analysis (Figs. 5 and 6), we observe that the motion trends become less pronounced due to the absence of the secondary modulation instability band. Nevertheless, in this case, the two components still exhibit distinct motion patterns and maintain reverse symmetry. The reason behind this phenomenon remains consistent with the previous situation. However, since there are only two branches of modulation instability, the system consistently resides near the quasi-momentum space of the main modulation instability band once the wave function enters chaotic oscillation.

**Conclusions**    We delve into the examination of modulation instability and its consequential dynamic patterns in one-dimensional two-component Bose-Einstein condensates with spin-orbit coupling. The study reveals the existence of four distinct zero momentum states within the system, where two of them carry currents while the remaining two do not under specific conditions. It should be noted that the generation of these four states is not solely determined by spin-orbit coupling; however, the presence of spin-orbit coupling does impact the modulation instability of the system. Previous research predominantly focuses on the zero quasi-momentum state without current carrying, neglecting the investigation of the zero quasi-momentum state with current carrying. We specifically explore the modulation instability of current-carrying zero momentum states. The findings indicate that in the presence of Rabi coupling, when the intra-component interaction surpasses the inter-component interaction, the modulation instability image manifests four branches, consisting of two main modulation instability bands and two secondary modulation instability bands. Conversely, when the intra-component interaction is lower than the inter-component interaction, the modulation instability image presents only two branches. We also establish a correlation between modulation instability and the nonlinear dynamic evolution of the system. Additionally, the presence of modulation instability can trigger the emergence of intricate patterns.

**Key words**    atomic and molecular physics; spin-orbit coupling; Bose-Einstein condensate; modulation instability